SPUR GOLD PROJECT, CARGO DISTRICT, NEW SOUTH WALES: HYDROTHERMAL ALTERATION AND GOLD MINERALISATION IN A TELESCOPED PORPHYRY–EPITHERMAL SYSTEM, MACQUARIE ARC

Jessica Askew[1,2], Malai Ila'ava[1,2,3], S. Meffre[2], T. Wells[2], Y. Cajal Contreras[2], D.R. Cooke[2], and P. Duerden[1]

[1] Waratah Minerals

[2] CODES – University of Tasmania

[3] Ila'ava Lava

Key Words: Spur, Cargo, epithermal gold, hydrothermal alteration, gold mineralisation, pyrite trace elements, telescoped porphyry–epithermal system, Macquarie Arc, Molong Volcanic Belt

INTRODUCTION

The Cargo Cu–Au system, in the Molong Volcanic Belt of the Late Ordovician Macquarie Arc, comprises porphyry-style Cu–Mo mineralisation at depth and superimposed epithermal gold in the overlying volcanic wallrock, a telescoped porphyry–epithermal system in which gold is concentrated at the epithermal level. It forms the Spur Gold Project (EL5238) of Waratah Minerals Limited (ASX:WTM), 5 km west of the Cadia Valley operations in central New South Wales, over the historic Consols and Ironclad goldfields; the project is at exploration stage, with no Mineral Resource estimated. Building on the volcanic and intrusive characterisation of Askew et al. (in prep.), this contribution describes the hydrothermal alteration, gold mineralisation, and pyrite trace-element chemistry of the epithermal system and their relationship to the porphyry environment.

The highest-grade gold in the Macquarie Arc is hosted in the wallrock of porphyry and epithermal systems, as at Ridgeway, Cadia East, Cowal, and Boda, rather than within the intrusive centres that earlier exploration at Cargo targeted; Spur tests that wallrock position.

GEOLOGICAL SETTING

The Macquarie Arc is a dismembered Ordovician to earliest Silurian intra-oceanic arc, preserved as four fault-segmented volcanic belts in the eastern Lachlan Orogen and accreted to Gondwana during the Benambran Orogeny (Crawford et al., 2007; Glen et al., 2012). It contains more than 83 Moz Au and 17.2 Mt Cu (recalculated from Kreuzer et al., 2015) and evolved from basaltic–andesitic sequences to calc-alkaline and locally shoshonitic suites (Cooke et al., 2007).

At Cargo, gold is hosted by the Cargo Volcanics, a submarine succession of Fe-rich, mafic–intermediate lavas and volcaniclastic rocks (Simpson et al., 2007), intruded by the multiphase Cargo Intrusive Complex (monzodiorite to quartz monzonite, with dacite porphyries) emplaced between 471 and 466 Ma (U–Pb zircon; Askew et al., in prep.); its magmatic affinity, calc-alkaline or alkalic, is unresolved. Molybdenite Re–Os ages of 469.8–471.6 Ma and a magmatic–hydrothermal pulse at 466–467 Ma constrain the main mineralising interval. Intrusion, mineralisation, and alteration follow a northwest-trending corridor along a reactivated segment of the Molong Lineament, and the system was later offset by the Essex, Tywi, and Cothi faults.

DEPOSIT GEOLOGY

Gold at Spur occupies a near-surface epithermal corridor, the Spur Gold Corridor and the Consols Zone, in altered basalt and albitised andesite along the margins of the intrusive complex, telescoped onto porphyry-style mineralisation; geophysical and drilling data indicate several intrusive centres rather than a single porphyry. The Consols envelope exceeds 400 m (E–W), 500 m (N–S), and 600 m (vertical) and contains three intercepts of more than 200 g·m Au. Lodes are steep to subvertical (75–80% of true width); grades increase toward syn-mineral monzonite and monzodiorite contacts, whereas post-mineral dykes dilute and truncate ore.

Representative intercepts include 81 m at 2.42 g/t Au from 536 m (Consols, SPD048), 208.7 m at 1.17 g/t Au from 514 m (incl. 38 m at 3.61 g/t Au; Spur, SPRCD062), and 11 m at 10.82 g/t Au from an oxidised skarn at Spur East (SPRC002).[1]

MINERALISATION AND ALTERATION

Gold occurs in several styles: dominant epithermal stringer and lode gold in the Spur and Consols corridors, hosted in altered basalt and albitised andesite; subordinate oxidised skarn (hematite–epidote–pyrite ± magnetite) at Spur East; siliceous stockwork at Spur South; and, at depth, porphyry-style Cu–Au (chalcopyrite ± bornite in A/B veins and potassic magmatic-hydrothermal breccia) at Breccia West. The ore assemblage is pyrite-dominant, with chalcopyrite, minor bornite, and magnetite; gold occurs as free gold, inclusions in chalcopyrite, electrum, and with bismuth tellurides, silver is minor, and molybdenum increases at depth toward the porphyry (Fig. 1).

Gold occupies a multi-stage, reactivated vein sequence logged in oriented core. Early porphyry-stage quartz–magnetite (A-type) and quartz (B-type) veins are overprinted by gold-stage pyrite–chalcopyrite–gold veins with potassic selvages, with quartz–carbonate–pyrite–chalcopyrite (± Au ± bismuthinite), pyrite–quartz–carbonate–chlorite–magnetite–gold, and late-carbonate assemblages. Chlorite–pyrite crackle breccias and the potassic magmatic-hydrothermal breccia of the Breccia West Cu–Mo zone accompany the veins; the highest grades occur where vein sets intersect and early veins are reactivated.

Alteration is zoned and overprinted, intensifying from weakly propylitic distal rocks to near-complete replacement in the most proximal, mineralised units. At depth, potassic (K-feldspar–quartz) and sodic-calcic to calcic (actinolite–albite–magnetite) assemblages with a Cu–Mo signature mark the porphyry (Breccia West, Dalcoath), overprinted by phyllic (quartz–sericite–pyrite) and locally argillic alteration. Outward and upward, the wallrock carries albite and magnetite (skarn) alteration passing into propylitic (chlorite–epidote–carbonate) assemblages, with silica–hematite–pyrite stringers at the shallowest levels. The downward potassic–calcic (Cu–Mo) and upward phyllic–silica–hematite–pyrite transitions vector toward the porphyry and epithermal environments respectively.

PYRITE TRACE-ELEMENT CHEMISTRY

LA-ICP-MS mapping of pyrite (20 mounts, 32 maps) across Spur, Breccia West, and Dalcoath resolves two populations that mirror the telescoped architecture (Fig. 2; cf. Sykora et al., 2018). Porphyry-environment pyrite (Breccia West and deeper holes) is Co–Ni–Se-rich (Co ~200–1000 ppm, locally >10,000 ppm; Se 20–80 ppm) with low As (<~100 ppm), whereas epithermal-corridor pyrite (Spur; e.g. SPRCD062) is As-rich (300–1300 ppm, locally ~7600 ppm) with elevated Sb, Tl, Ag, and Au. Maps of composite grains (SPRCD062; up to ~42 ppm Au, ~7600 ppm As) show gold concentrated in As–Te–Bi-rich domains, consistent with the bismuth-telluride association seen petrographically (Fig. 3-5). This porphyry-to-epithermal trend in pyrite provides an independent geochemical vector that reinforces the alteration and vein evidence for telescoping.

GOLD DEPORTMENT – CURRENT KNOWLEDGE

Initial gold deportment work at the Spur Zone involving uXRF scanning, petrology and gravity separation with sequential leaching on the gravity tails suggests that 90 to 97% of the gold can be recovered using a gravity circuit followed by conventional leaching process. Gravity separation recovered between 15 and 45% of gold with coarse gold grains in the gravity concentrate sizing up to 688um. Similar work is underway for the Consols Zone.[1]

DISCUSSION

The alteration zonation, vein paragenesis, and pyrite chemistry record a telescoped porphyry–epithermal system developed around a multiphase intrusive complex with multiple porphyry centres (Sillitoe, 2010). Telescoping is shown by gold-stage veins overprinting porphyry-stage A/B veins, phyllic–argillic alteration overprinting the potassic core, and the porphyry-to-epithermal trend in pyrite. Porphyry-style mineralisation at depth (potassic–calcic alteration, Cu–Mo, magnetite–quartz–chalcopyrite veins; Breccia West) marks where the intrusive centres exsolved oxidised, metal-bearing magmatic fluids; gold was deposited where these fluids ascended into the epithermal environment and reacted with Fe-rich wallrock, cooling, oxidising, and sulphidising the mafic host. The alteration assemblages, vein sets, and pyrite compositions therefore vector toward both the shallow gold and the deeper porphyry centres.

Sulphur-isotope data are consistent with this model, with sulphide $\delta^{34}S$ of −9.7 to +1.9‰ (n = 163) recording a magmatic sulphur source and the most negative values consistent with epithermal-stage boiling (Askew, in prep.). Cargo is an evolving target: continued drilling and analysis refine its alteration and mineralisation framework, and the magmatic affinity of the complex and the position of the fault-offset porphyry centres remain open questions.

ACKNOWLEDGEMENTS

We thank Waratah Minerals Limited for permission to publish and for access to its drilling, assay, and geophysical datasets, and we are grateful to the Waratah Minerals geology team, whose field, logging, and technical support made this work possible. We thank the CODES team at the University of Tasmania for the analytical facilities, training, and discussion that underpin this study, and Jessica Askew warmly thanks her supervisors for their guidance and mentorship throughout her doctoral research. Exploration results are reported under the JORC Code (2012), with Mr Peter Duerden (RPGeo, AIG) as Competent Person.

[1] Intercepts reported by Waratah Minerals Limited (ASX:WTM) under the JORC Code (2012); Competent Person P. Duerden (RPGeo, AIG). Grades are length-weighted, uncut, at a 0.1 g/t Au lower cut with up to 5 m internal dilution; intervals are downhole lengths (estimated >75–80% of true width for subvertical zones). ASX:WTM releases, 2024–2026.

REFERENCES

COOKE D.R., WILSON A.J., HOUSE M.J., WOLFE R.C., WALSHE J.L., LICKFOLD V., & CRAWFORD A.J., 2007, Alkalic porphyry Au–Cu & associated mineral deposits of the Ordovician to Early Silurian Macquarie Arc, New South Wales: Australian Journal of Earth Sciences, v. 54, p. 445–463.

CRAWFORD A.J., MEFFRE S., SQUIRE R.J., BARRON L.M., & FALLOON T.J., 2007, Middle & Late Ordovician magmatic evolution of the Macquarie Arc, Lachlan Orogen, New South Wales: Australian Journal of Earth Sciences, v. 54, p. 181–214.

GLEN R.A., QUINN C.D., & COOKE D.R., 2012, The Macquarie Arc, Lachlan Orogen, New South Wales: its evolution, tectonic setting & mineral deposits: Episodes, v. 35, p. 177–186.

KREUZER O.P., MILLER A.V.M., PETERS K.J., PAYNE C., WILDMAN C., PARTINGTON G.A., PUCCIONI E., MCMAHON M.E., & ETHERIDGE M.A., 2015, Comparing prospectivity modelling results & past exploration data: A case study of porphyry Cu–Au mineral systems in the Macquarie Arc, Lachlan Fold Belt, New South Wales: Ore Geology Reviews, v. 71, p. 516–544.

REICH M., KESLER S.E., UTSUNOMIYA S., PALENIK C.S., CHRYSSOULIS S.L., & EWING R.C., 2005, Solubility of gold in arsenian pyrite: Geochimica et Cosmochimica Acta, v. 69, p. 2781–2796.

SILLITOE R.H., 2010, Porphyry copper systems: Economic Geology, v. 105, p. 3–41.

SIMPSON C.J., SCOTT R.J., CRAWFORD A.J., & MEFFRE S., 2007, Volcanology, geochemistry & structure of the Ordovician Cargo Volcanics in the Cargo–Walli region, central New South Wales: Australian Journal of Earth Sciences, v. 54, p. 273–300.

SYKORA S., COOKE D.R., MEFFRE S., STEPHANOV A.S., GARDNER K., SCOTT R., SELLEY D., & HARRIS A.C., 2018, Evolution of pyrite trace element compositions from porphyry-style & epithermal conditions at the Lihir gold deposit: Implications for ore genesis & mineral processing: Economic Geology, v. 113, p. 193–208.

FIGURES

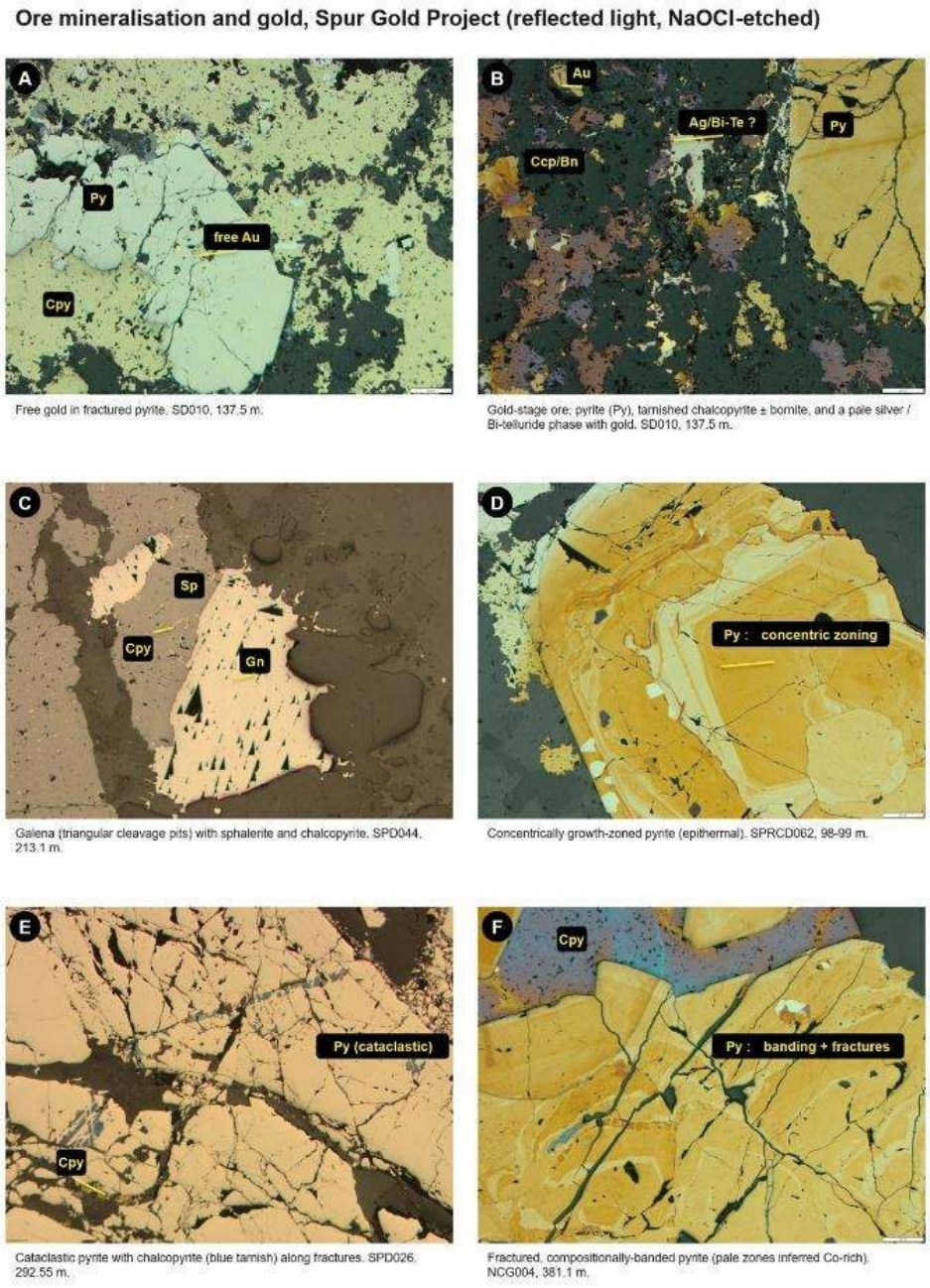

Figure 1. Ore and gold, Spur Gold Project (reflected light, NaOCl-etched): (A) free gold in fractured pyrite (SD010, 137.5 m); (B) gold-stage pyrite, chalcopyrite ± bornite, and a silver/Bi-telluride phase with gold (SD010, 137.5 m); (C) galena with sphalerite (SPD044, 213.1 m); (D) concentrically zoned epithermal pyrite (SPRCD062, 98–99 m); (E) cataclastic pyrite with fracture-controlled chalcopyrite (SPD026, 292.55 m); (F) fractured, compositionally banded pyrite (NCG004, 381.1 m). Scale bars 200 µm; identifications optical, chalcopyrite–bornite and silver/Bi-telluride phases to be confirmed by SEM-EDS.

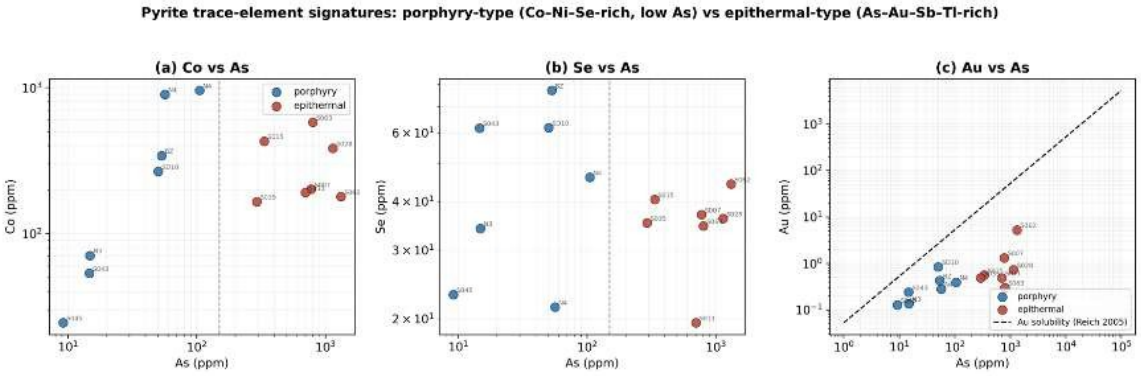

Figure 2. Pyrite trace-element discrimination (LA-ICP-MS, LADR-quantified; geometric-mean concentrations, one point per mount): (a) Co vs As, (b) Se vs As, (c) Au vs As. Porphyry-type pyrite (Co–Ni–Se-rich, low As; blue) is separated from epithermal-type pyrite (As–Au–Sb–Tl-rich; red). Dashed line in (c) is the gold solubility limit of Reich et al. (2005); nearly all pyrite plots below it, indicating lattice-bound gold.

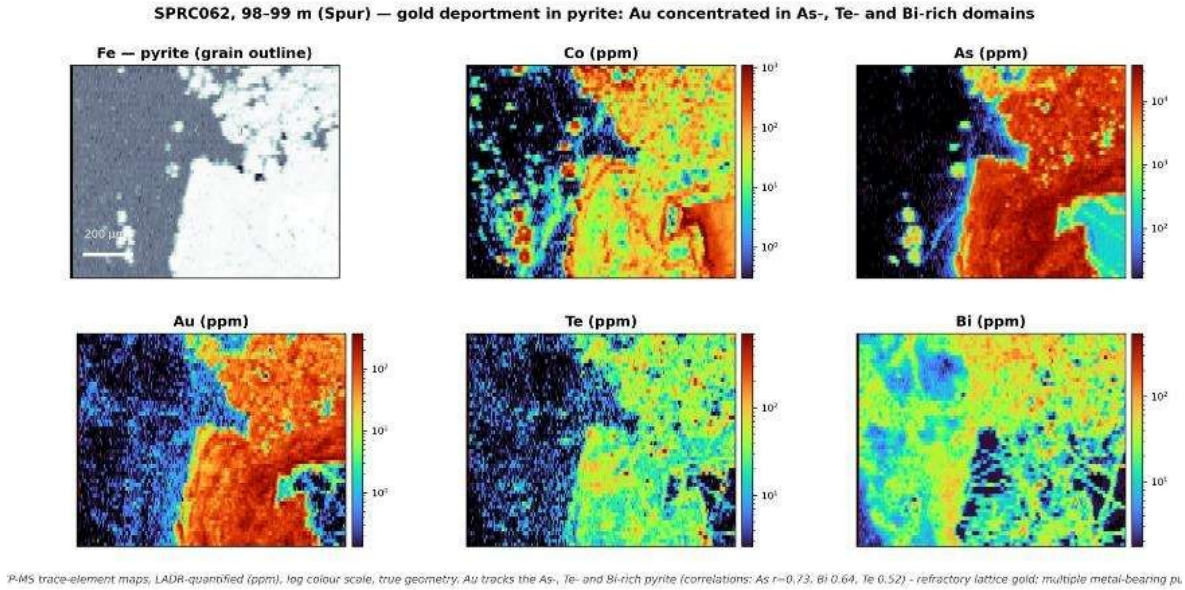

P-MS trace-element maps, LADR-quantified (ppm), log colour scale, true geometry. Au tracks the As-, Te- and Bi-rich pyrite (correlations: As r=0.73, Bi 0.64, Te 0.52) - refractory lattice gold; multiple metal-bearing pu

Figure 3. LA-ICP-MS maps of gold-bearing composite pyrite (SPRCD062, 98–99 m, Spur), in ppm (log colour scale). Fe outlines the pyrite; Co, As, Au, Te, and Bi show gold concentrated in As–Te–Bi-rich domains. Scale bar 200 µm.

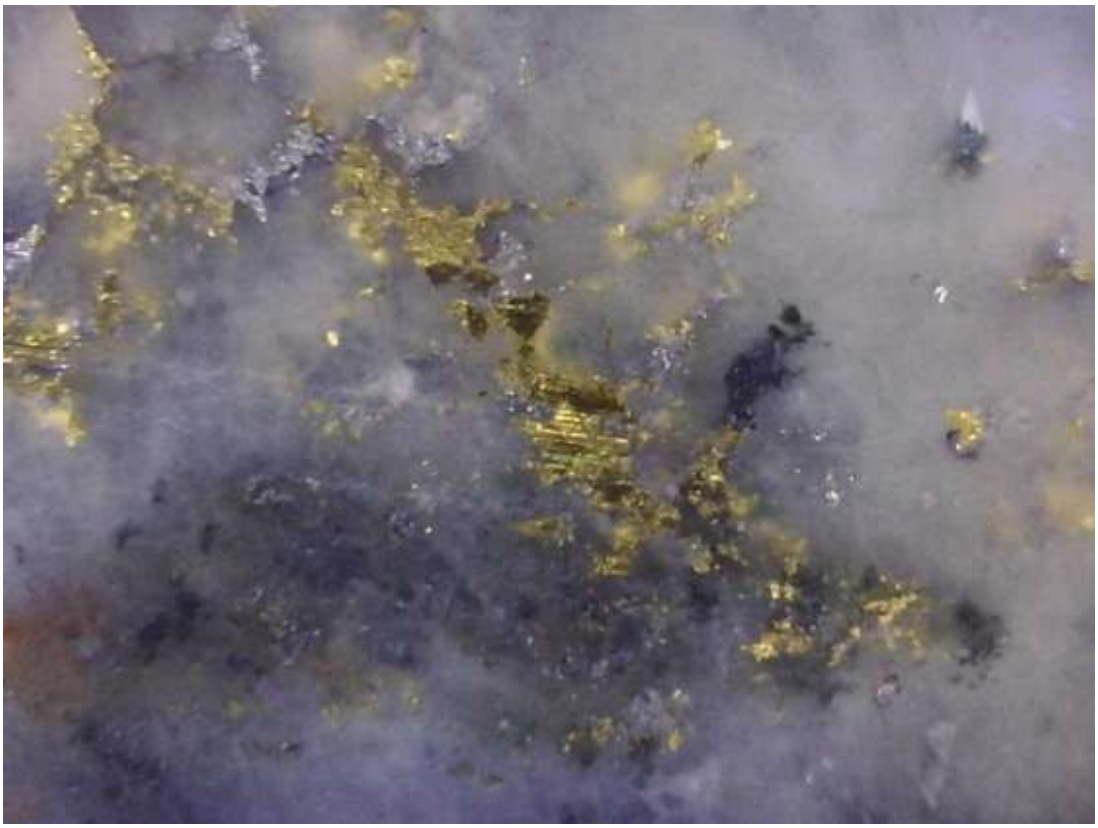

Figure 4. Visible gold, SPD021@330m FOW 10mm.

Figure 5. Visible gold with Bi-tellurides. SPD058 @ 43.3m. FOW 10mm.